

Simulation of Sloshing Effects in Cylindrical Containers under Seismic Loading

Sami A. Kilic¹, Zuhail Ozdemir²

Assistant Professor¹, Bogazici University, Kandilli Observatory, Dept. of Earthquake Engineering, Cengelkoy 34684, Istanbul, Turkey, e-mail: skilic@boun.edu.tr

Ph.D. Candidate², Bogazici University, Kandilli Observatory, Dept. of Earthquake Engineering, Cengelkoy 34684, Istanbul, Turkey, e-mail: zuhal.ozdemir@boun.edu.tr

Summary:

Past experience has shown that metal cylindrical containment tanks undergo significant damages during strong earthquakes. The main design code widely adopted for these tanks is the American Petroleum Institute's API-650 code [1]. The basis of this design code dates back to 1978 [2], and uses simplified procedures to estimate the hydrodynamic loads induced during earthquakes. The damage observed for the cylindrical tanks raises questions about the adequacy of the API-650 code for seismic applications.

This study employs the ALE modeling techniques of LS-DYNA in order to simulate the dynamic response of rigid rectangular and cylindrical tanks under the ground motion recorded during the 17 August 1999 Marmara earthquake in Turkey.

Keywords:

Liquid Storage Tanks, Sloshing, Earthquake, Hydrodynamic Response

1 Introduction

Observation of severe damage in cylindrical liquid storage tanks has been very widespread during the 1989 Loma Prieta (California, USA), the 1994 Northridge (California, USA), 1995 Kobe (Japan), and the 1999 Marmara (Turkey) earthquakes, among many others. Damage to liquid storage tanks may lead to fire, explosion, disruption of production, and environmental pollution. These consequences also result in large amounts of financial loss. Damage to free-standing cylindrical ground storage tanks during many earthquakes demonstrates the need for better understanding of the seismic behavior of these structures.

There is a wide variety of code guidelines for the earthquake resistant design of steel liquid storage tanks. The API-650 code is worldwide for the seismic analysis and design of liquid containment tanks. Although numerous analytical, experimental, and numerical works have been carried out in recent years, the API-650 code is based on the analytical work carried out by Housner in 1954 [3].

In this study, field observations related to damage of liquid storage tanks during the Marmara earthquake is provided in order to show the seismic behavior of such structures. Available formulations to simulate dynamic analysis of fluid-structure coupled systems in LS-DYNA are summarized. Three-dimensional rectangular and cylindrical rigid tank models are developed. Fluid-structure interaction responses of the tanks are evaluated using the explicit time-integration capabilities of the LS-DYNA code.

2 Observed Tank Damages during the 1999 Marmara Earthquake

The Marmara earthquake struck a region with densely populated heavy industrial facilities on 17 August 1999 with a moment magnitude of 7.4 (M_w). The earthquake caused significant structural damages to petrochemical containment tanks at the Tupras Refinery. Sloshing actions of combustible liquid inside the tanks deformed the tank roofs and upper tank walls as shown in Fig. 1. Insufficient freeboard in fixed-roof tanks may result in plate buckling type of damages at the roof level. Roof-shell junction of the tanks ruptured due to excessive joint stresses as illustrated in Fig. 2. Deformation of the tank shell caused the separation of the piping connections. Sloshing in the tanks led to the combustion of the contents (liquid naphtha) and resulted in an extensive fire in the tank farm location. Fig. 3 shows deformed state of burned tanks. Leakage of chemicals and hazardous materials from the damaged tanks led to environmental pollution at the refinery. The petrochemical facilities in the area experienced extensive losses and business disruption.



Fig. 1 : Deformation of cylindrical tank with fixed roof after the 17 August 1999 Marmara Earthquake at the Tupras Refinery.



Fig. 2: Separation of roof-wall junction of a cylindrical tank with fixed roof



Fig. 3: Post-earthquake fire damage of the naphtha tanks at the Tupras Refinery

3 Fluid-Structure Interaction Formulations in LS-DYNA

LS-DYNA allows the user to simulate the dynamic response of fluid-structure coupled systems using pure Lagrangian, coupled Lagrangian and Eulerian, and Smooth Particle Hydrodynamics (SPH) methodologies.

The Lagrangian formulation is available in LS-DYNA for the analysis of the behavior of fluid and structure. The interaction between fluid and structure was modeled using the contact algorithm where the fluid was defined as the slave part. Using the Lagrangian approach to describe the dynamic behavior of a fluid, the Lagrangian mesh follows the fluid material. If the fluid material undergoes large distortions, it will lead to a significant increase in CPU time and, in the worse case, to premature analysis termination. The advantage of the Lagrangian approach is that the free surface of the material is automatically captured by the mesh. The main disadvantage of the Lagrangian approach arises from the fact that problems develop in physical situations that involve highly deformed fluid surfaces. Only a single fluid material can be modeled in each Lagrangian element. In addition, fluid separation can not be modeled

Eulerian formulation provides an alternative for fluid modeling in LS-DYNA. In the Eulerian formulation the mesh is stationary in space and the material flows through the mesh by advection. The Eulerian approach originated from the computational fluid dynamics field and is best suited for large deformation fluid flow problems. The disadvantage of the Eulerian approach is that a fine mesh is required to capture the material response, making the method very computationally expensive.

The Arbitrary Lagrangian-Eulerian (ALE) approach is another alternative for simulating large deformation problems in LS-DYNA. In its most basic sense, the ALE method assumes that the mesh motion is independent of the motion of the material being analyzed. Although the mesh motion may be arbitrary, it typically deforms with the material in the near-Lagrangian flow fields. The greatest advantage of the ALE method is that it allows smoothing of a distorted mesh without performing a complete remesh. This smoothing allows the free surface of the material to be followed automatically without encountering the distortional errors of the Lagrangian approach. Due to the path dependence, the relative motion between the mesh and the material must be taken into account in the material constitutive equations. The ALE method is best suited for problems for which the material flow is relatively predictable.

Another option to analyze fluid-structure coupled problems in LS-DYNA is the Smooth Particle Hydrodynamics (SPH) method, which is a mesh-less Lagrangian technique used to model the fluid equations of motion. Particles in the SPH method carry information about their hydrodynamic and thermo-dynamic behavior, in addition to mass conservation. The SPH method allows modeling of large fluid dispersions without the expense of volumetric meshing using solid elements. Due to the absence of a grid, this method allows solving many problems that are hardly reproducible in other classical methods and solves the problem of large mesh deformations. Another advantage of the SPH method is that due to the absence of a mesh, problems with irregular geometry can be solved. A large number of particles are needed for the SPH calculations. The SPH method is computationally demanding, both in terms of memory and CPU time.

4 Finite Element Model Used in Simulation Studies

In this study, the seismic responses of three-dimensional rectangular and cylindrical tanks have been analyzed. Liquid material in the tank is modeled using the Eulerian approach. The remaining portion of the Eulerian mesh is filled with gas (air). The tank enclosure is modeled with Lagrangian shell elements and is assumed to be rigid in this study. The nodes at the interface between the Eulerian and the Lagrangian parts are shared (merged nodes). The cylindrical tank has a radius of 7.50 m and a total height of 6.00 m. The rectangular tank dimensions are 15.00 m x 10.16 m x 7.11 m. Water ($\rho = 1000 \text{ kg/m}^3$) is filled up to a height 3.56 m in the rectangular tank model, and up to 3.00 m for the cylindrical model. Both tanks are made of steel with a density of 7800 kg/m^3 and elastic modulus of 2.00 GPa. The tank enclosures are modeled with Belytschko-Tsay shell elements. The thickness of the tank shell is 0.051 m. Water and air are modeled with Eulerian solid elements using the *MAT_NULL model. The *EOS_LINEAR_POLYNOMIAL is used for air and water. Tanks are considered to be rigid and fully anchored to the base. The command *ALE_REFERENCE_SYSTEM_GROUP is utilized to allow mesh motion for the Eulerian elements.

In the rectangular tank model, the Eulerian mesh consists of 8400 solid elements with a typical edge length of 0.50 m, and the Lagrangian mesh consists of 2600 shell elements with a typical edge length of 0.50 m. The model contains 9765 nodes. The cylindrical tank model has 1869 nodes, 746 shell elements for the tank enclosure, and 1460 solid elements for the Eulerian mesh.

The models are loaded with gravity ($g = 9.81 \text{ m/sec}^2$) with *LOAD_BODY_Z. We apply the gravity body load in a ramp function. Nonlinear dynamic time history analyses are performed for rectangular and cylindrical tanks under bi-directional horizontal earthquake motions (E-W and N-S components) recorded during the 17 August 1999 ($M_w=7.4$) Marmara earthquake at the YPT ground station. In addition, the vertical component is also combined with the bi-directional components in separate analyses in order to assess the effect of the vertical motion. The acceleration time history, the acceleration response spectrum, and the displacement response spectrum of the YPT record are shown in Figs. 4 to 6. Particle trace of the bi-directional components of the YPT ground motion (the East-West and the North-South components) is illustrated in Fig. 7. Explicit dynamic analyses are carried out by using the single-precision LS-DYNA version 971.7000.129 on an Intel Core2Duo 2.00 GHz personal computer. The time step size and the total CPU time of the simulations are given in Table 1.

Table 1: Time step and total CPU time of the simulations

Tank Type	Rectangular Tank		Cylindrical Tank	
	EW-NS	EW-NS-UD	EW-NS	EW-NS-UD
Time step	6.32 E-5 second	6.34 E-5 second	3.81 E-5 second	3.81 E-5 second
Total CPU time	28230 seconds (7 hr 50 min)	16163 seconds (4 hr 29 min)	10948 seconds (3 hr 2 min)	10954 seconds (3 hr 2 min)

5 Results and Discussions

The API 650 design code provides an approach for determining the maximum sloshing wave height as a function of the sloshing period, the sub-soil classification, the peak ground acceleration, and the importance factor. The first sloshing period is also defined by an empirical formula, which is a function of the tank diameter and the depth of the liquid content. In the first part of this study, the height of the sloshing wave above the product design level is examined for rectangular and cylindrical tanks that are subjected to the East-West and the North-South components of the YPT ground motion records. In the second part, the tanks are subjected to all three components of the YPT records; namely the East-West, the North-South, and the vertical components (Up-Down). Liquid sloshing displacements obtained from simulations for cylindrical tanks are compared with the predictions of the API 650 code.

The sloshing period of the cylindrical tank investigated in this study is calculated as 5.09 seconds according to the API 650 formula. When applying the API 650 formula, it is assumed that the cylindrical tank belongs to Seismic Use Group II, is on site class C (medium soil). Free surface displacements are obtained as 0.62 m (East-West direction), 0.81 m (North-South direction), and 0.65 m (Up-Down direction). An SRSS combination of these wave heights leads to 1.03 m. Maximum free surface wave heights for cylindrical and rectangular tanks observed from LS-DYNA simulations are given in Table 2. Comparison of the maximum free surface displacements of the cylindrical tank obtained from LS-DYNA simulations with API 650 predictions for both earthquake component combinations show that simulation results are in the permissible range per API 650 regulations. Simulation results also show that the effect of up-down component of earthquake on sloshing wave height for a rectangular tank is higher than for a cylindrical tank.

Relative positions of the rectangular and cylindrical tanks under two different combinations of the Marmara earthquake ground motion components are given in Figs. 8 to 11. The displacements of the

Lagrangian tank shell are magnified 5 times in order to better illustrate the bi-lateral motion of the tank under seismic action.

Further simulations should be carried out in order to assess the adequacy of the API 650 code for calculating sloshing wave heights. A deformable tank shell may lead to higher wave height in terms of sloshing. A combination of insufficient freeboard and an excessive sloshing wave height may lead to tank roof damage. In addition, different tank diameters and liquid depths should be investigated. Various ground motion record are also needed due to the fact that the sloshing results depend on the ground excitation.

6 Summary

In this study, the seismic sloshing responses of three-dimensional rectangular and cylindrical rigid tanks are investigated using LS-DYNA using an Eulerian approach. The two horizontal and the vertical components of the 17 August 1999 Marmara earthquake record at the YPT ground station are used in the nonlinear dynamic time history analyses. The API 650 tank design code predictions of maximum free surface displacement for the cylindrical tank are compared with the LS-DYNA simulation results. Preliminary calculations show that the sloshing wave heights of the simulations are within the limits of the API 650 code for the rigid tank assumption. Further studies are needed to assess the sloshing heights in flexible tanks.

Table 2. Wave height results obtained from the LS-DYNA simulations.

Tank Type	Rectangular Tank		Cylindrical Tank	
	EW-NS	EW-NS-UD	EW-NS	EW-NS-UD
Earthquake Component				
Maximum Surface Displacement (m)	0.76	0.96	0.24	0.25

7 Acknowledgements

The authors express their deepest gratitude to Professor Mhamed SOULI of Université des Sciences et Technologies de Lille (USTL). This work is supported by the Turkish Scientific and Research Organization Engineering Research Group (TUBITAK-MAG) through contract numbers 105M332 and 107M002, and the Bogazici University Research Fund (BAP) through contract numbers 06T102 and 07HT102.

8 References

- [1] API 650 : "Welded Storage Tanks for Oil Storage", American Petroleum Institute Standard, Washington D. C., 2003.
- [2] Wozniak R.S., and Mitchell W.W. : "Basis of Seismic Design Provisions for Welded Steel Oil Storage Tanks", American Petroleum Institute, 43rd Mid-year Meeting, Session on Advances in Storage Tank Design, Toronto, Canada, 1978.
- [3] Housner G.W. : "Earthquake Pressures on Fluid Containers", 8th Technical Report under Office of Naval Research, California Institute of Technology, Pasadena, California, August, 1954.
- [4] Kilic S. and Sozen M. : "An Evaluation of the Effect of the 17 August 1999 Marmara Earthquake on Two Tall Reinforced Concrete Chimneys", ACI Structural Journal, American Concrete Institute (ACI), Vol. 100, No. 3, pp. 357-364, May-June 2003.

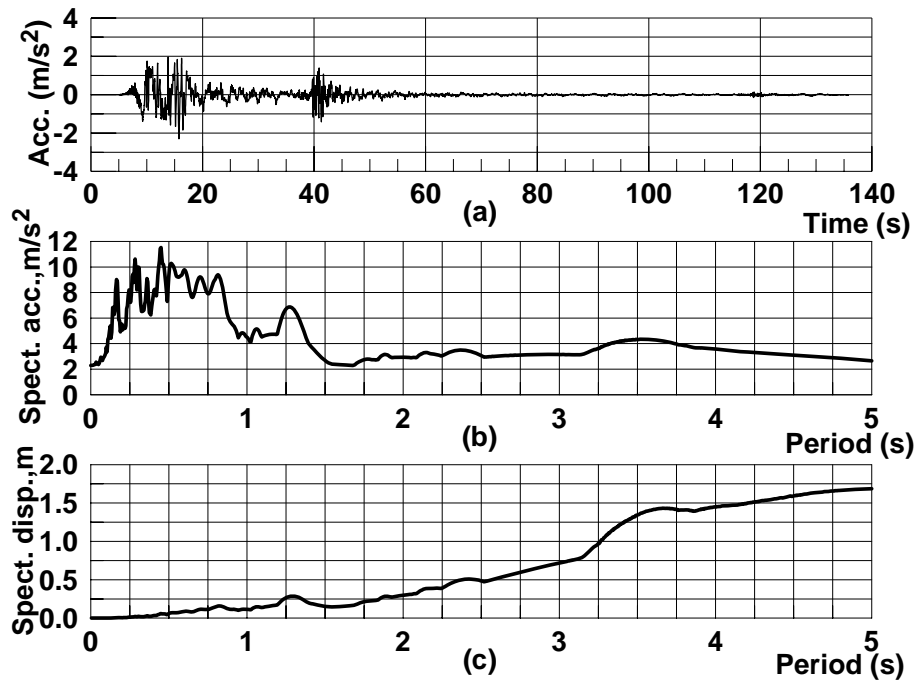


Fig. 4: The East-West acceleration record measured at the YPT station, and the linear acceleration/displacement responses calculated for a damping factor of 2% of critical [4].

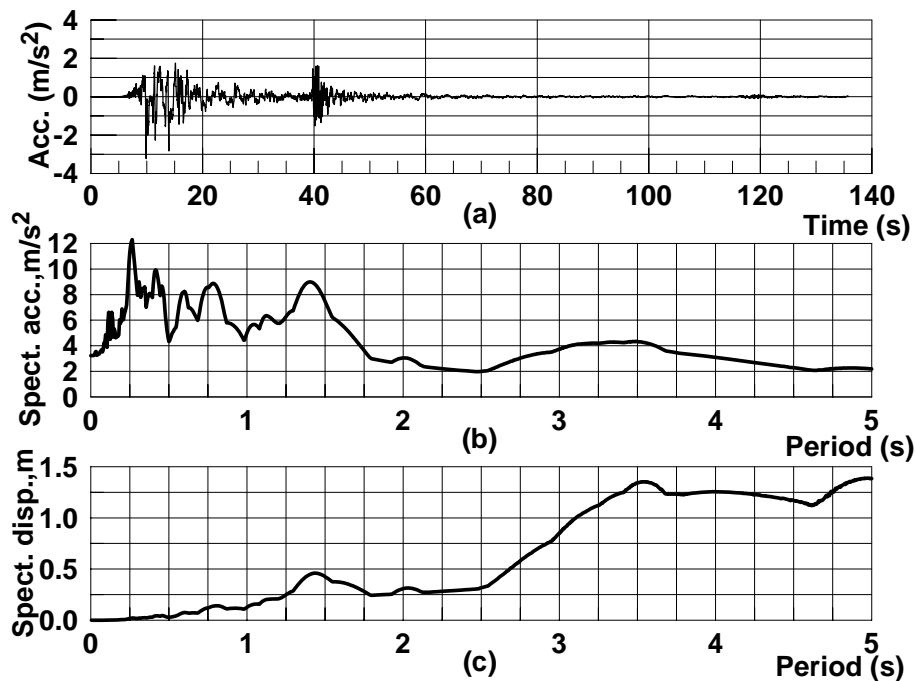


Fig. 5: The North-South acceleration record measured at the YPT station, and the linear acceleration/displacement responses calculated for a damping factor of 2% of critical [4].

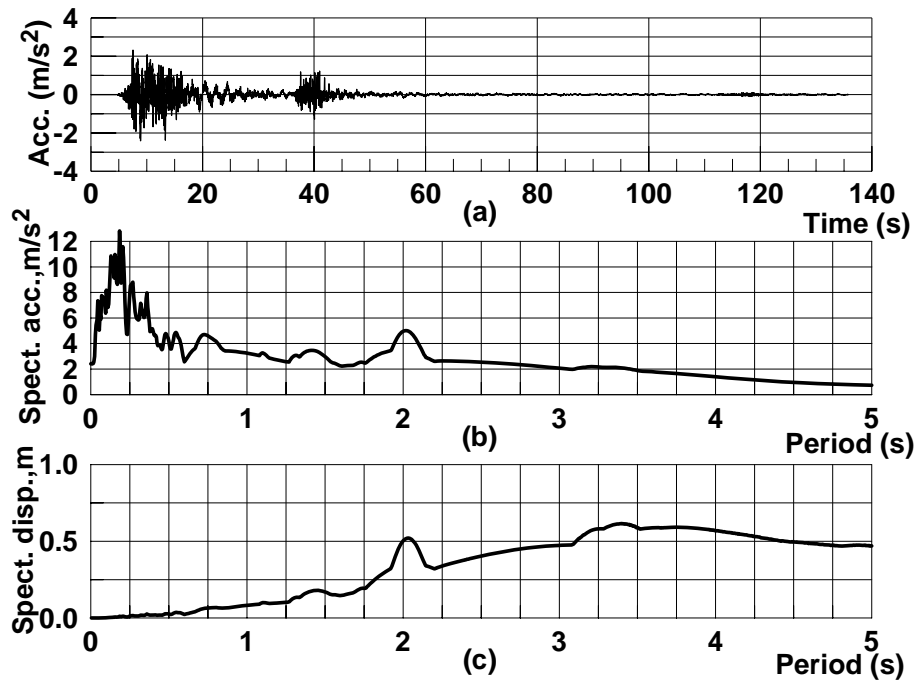


Fig. 6: The Up-Down acceleration record measured at the YPT station, and the linear acceleration/displacement responses calculated for a damping factor of 2% of critical [4].

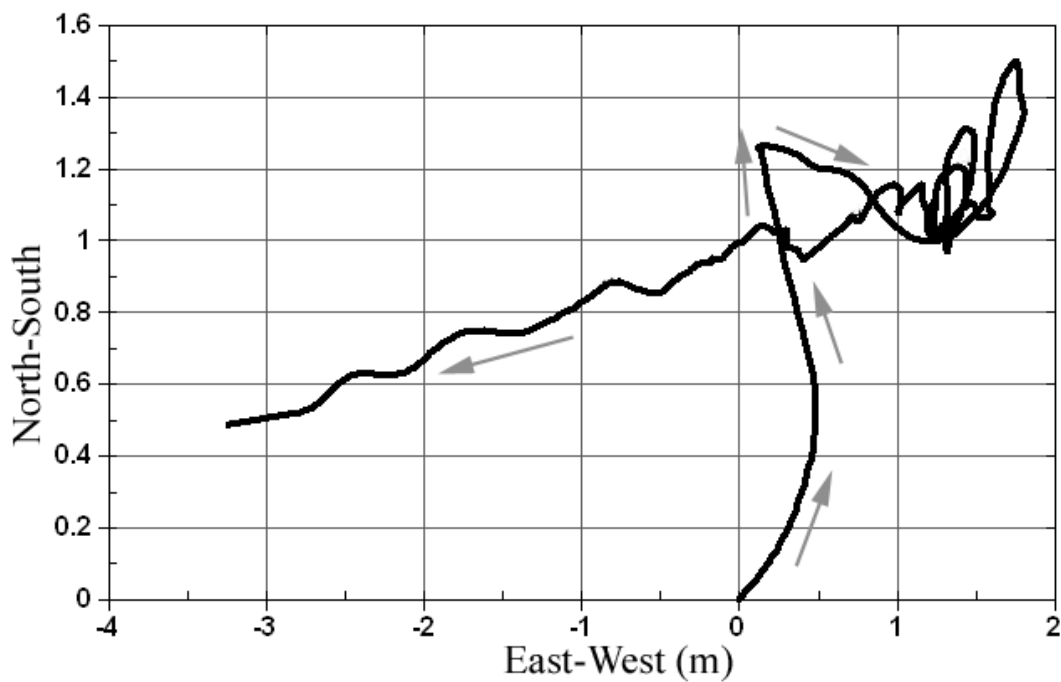


Fig. 7: Particle trace of the bi-directional components of the YPT ground motion.

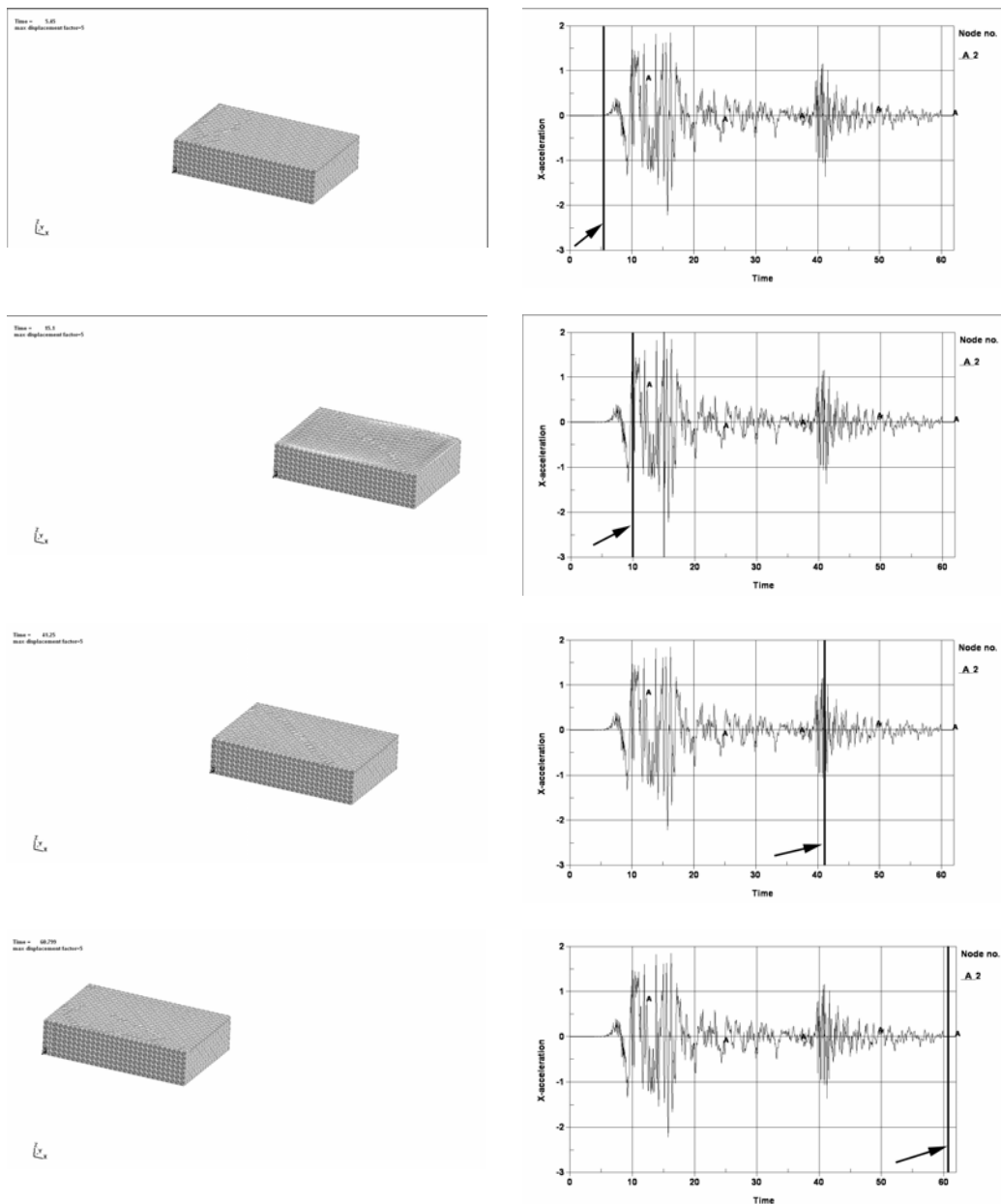


Fig. 8: Relative positions of the rectangular tank (displacements magnified 5 times) and the corresponding instances of the YPT East-West ground motion record (marked with an arrow along the timeline). Only the East-West and the North-South components of the YPT record are used in the analysis.

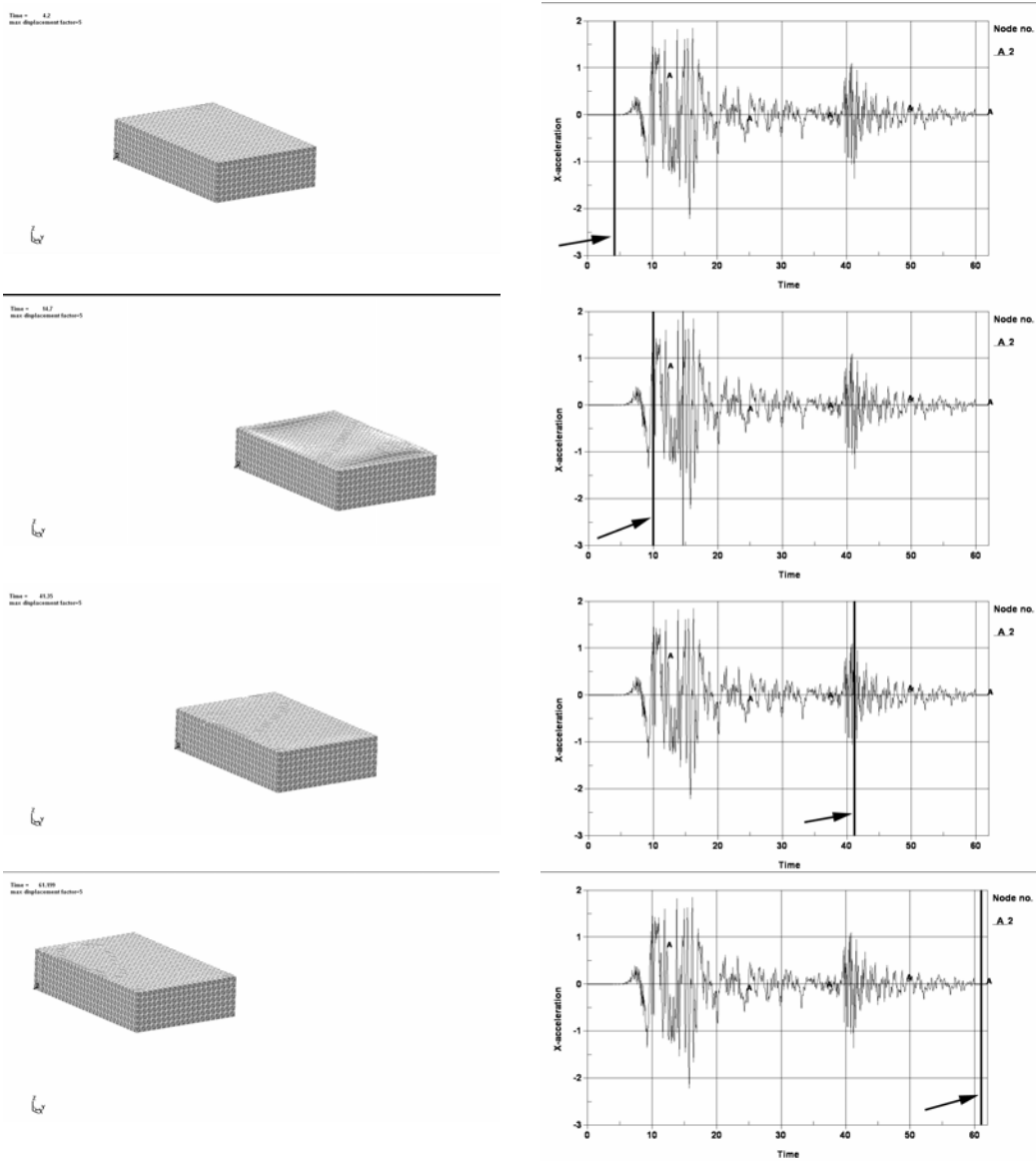


Fig. 9: Relative positions of the rectangular tank (displacements magnified 5 times) and the corresponding instances of the YPT East-West ground motion record (marked with an arrow along the timeline). The East-West, the North-South, and the Up-down components of the YPT record are used in the analysis.

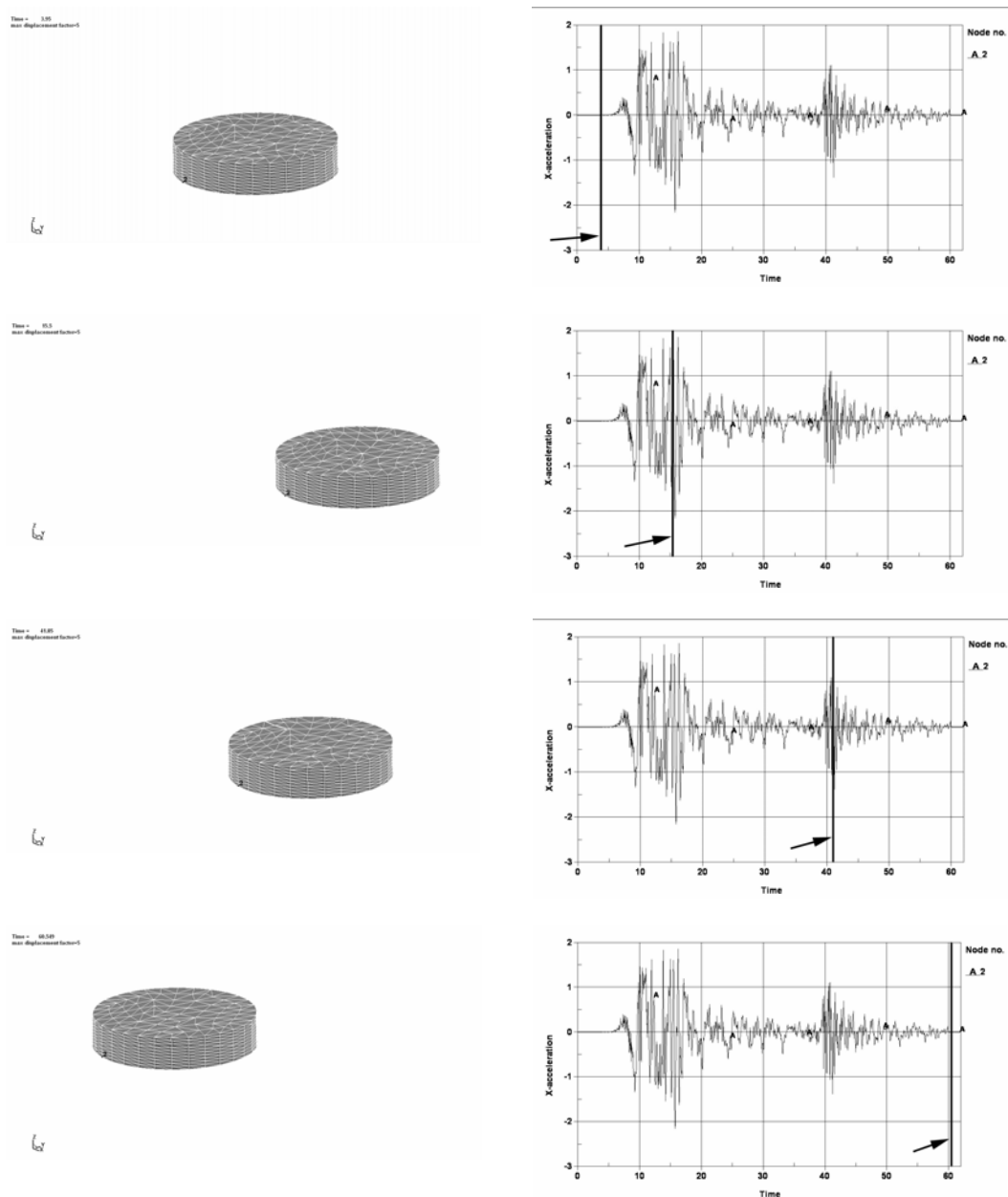


Fig. 10: Relative positions of the cylindrical tank (displacements magnified 5 times) and the corresponding instances of the YPT East-West ground motion record (marked with an arrow along the timeline). Only the East-West and the North-South components of the YPT record are used in the analysis.

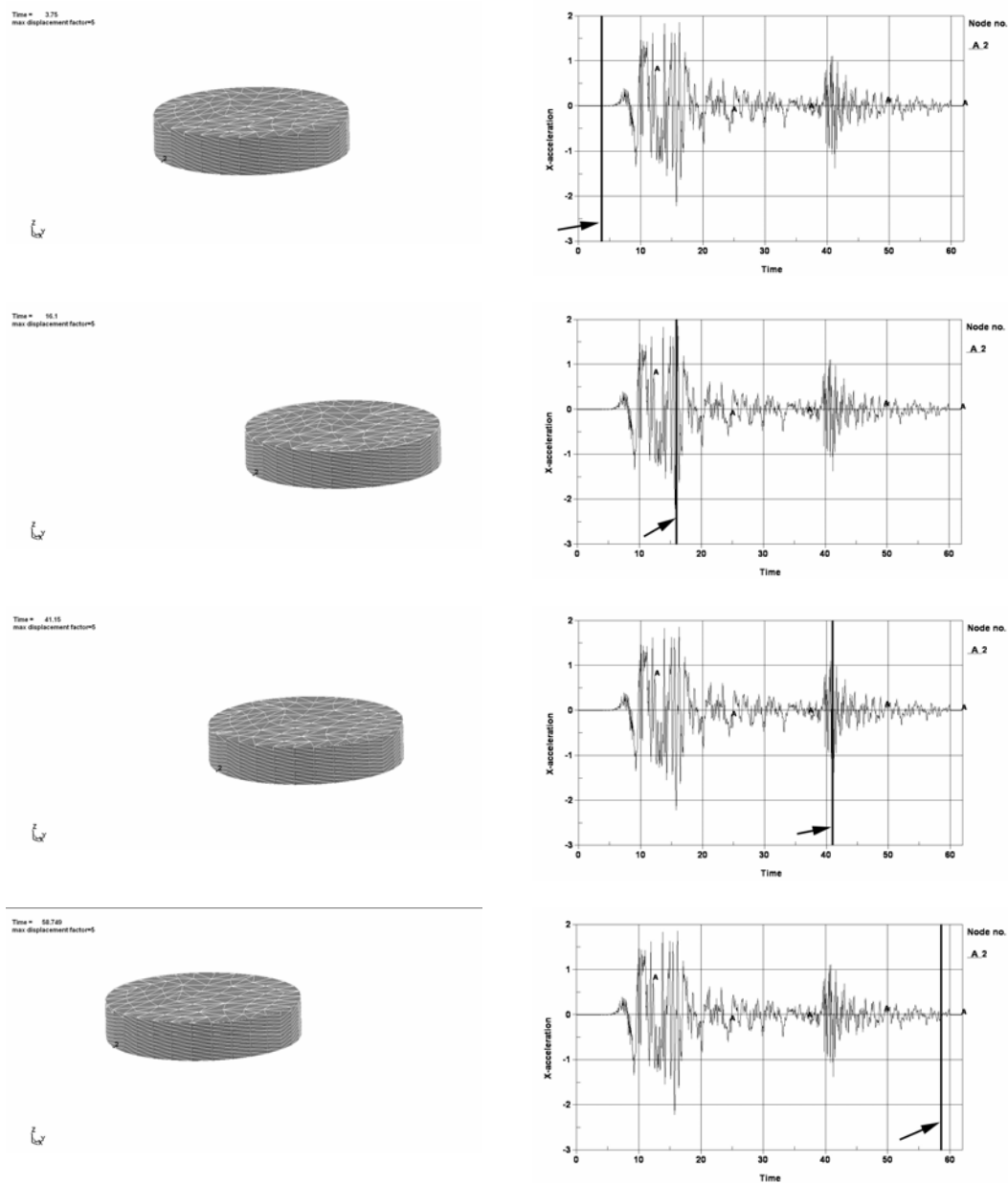


Fig. 11: Relative positions of the cylindrical tank (displacements magnified 5 times) and the corresponding instances of the YPT East-West ground motion record (marked with an arrow along the timeline). The East-West, the North-South, and the Up-down components of the YPT record are used in the analysis.